

Direct Numerical Simulation of Mixing Performance in Turbulent Channel Flow with an Elastic Cylinder

Koichi Tsujimoto¹, Makoto Takeuchi¹, Toshihiko Shakouchi¹, Toshitake Ando¹

¹Division of Mechanical Engineering
Graduate School of Engineering, Mie University, Tsu, 514-8507, Japan

Abstract

In the present paper in order to investigate the possibility of flow control using an elastic cylinder, we conduct a simulation of a finite-length elastic cylinder installed in a turbulent channel flow. For an elastic cylinder, the rigorous equation of motion for elastic continuum is solved with a finite volume method; the effect of existence of cylinder in the flow computation is taken into account using the immersed boundary method. From time averaged quantities, we demonstrate that the elastic cylinder modulates wake structures, heat transfer characteristics and mixing performance.

Introduction

Fluid-Structure Interaction (FSI) problem is concerned with in various research fields such as mechanical, aerospace, civil and medical engineering, and their accurate prediction and control are desired. In particular, since the wake of wall mounted cylinder is a common flow regime in above-mentioned problem, the detail of the flow has been aggressively investigated so far[8]. In this study, we pay attention to the flow control using flexible structures such as elastic cylinder for the above mentioned flows. To investigate the potentiality of the control in advance, both high accurate and stable computational scheme is needed so that the actual phenomena including turbulence is well predicted. Therefore, in order to analyze efficiently the fluid-structure interaction, we propose a weak-coupling method in which for flexible structures, the rigorous equations of motion are discretized with finite volume method, for flow computations, the finite difference method (FDM) is used and the flexible structures is reproduced via immersed boundary method[2, 4] in the flow computation. In the present paper, using the proposed scheme, a DNS of turbulent channel flow with a elastic cylinder is conducted. Compared to the rigid cylinder, the modification of turbulent flow due to the elastic motion of cylinder is demonstrated through the visualization of instantaneous and mean flow fields. Further in order to investigate heat transfer and mixing performance due to the elastic motion of cylinder, transport equations of passive scalar is solved as well as the momentum transfer. It turns out that the elastic cylinder modulates wake structure, heat transfer characteristics, and mixing performance.

Numerical Method

Finite Volume Method for Elastic Body

The dynamics of a elastic body based on the continuum model can be written by the conservation law of mass and momentum[9]

$$\frac{d\rho}{dt} = -\rho \frac{\partial u_i}{\partial x_i} \quad (1)$$

$$\rho \frac{du_i}{dt} = \frac{\partial \sigma_{ij}}{\partial x_j} \quad (2)$$

where ρ is the density, u_i is the velocity component. In the

present study, the constitutive equations are assumed to be a Hookean elastic body:

$$\sigma_{ij} = s_{ij} - p\delta_{ij} - q_{ij} \quad (3)$$

$$\dot{\epsilon}_{ij} = \left(\frac{\partial u_i}{\partial x_j} + \frac{\partial u_j}{\partial x_i} \right) \quad (4)$$

$$\frac{dp}{dt} = -K \text{tr}(\dot{\epsilon}) \quad \left(K = \frac{E}{3(1-2\gamma)} \right) \quad (5)$$

where s_{ij} is the stress deviator tensor ϵ_{ij} the strain tensor and $\dot{\epsilon}_{ij}$ the rate of strain. K is the bulk modulus q_{ij} the artificial viscosity tensor and p the pressure. $\text{tr}(\dot{\epsilon})$ is the trace of the strain tensor. K is written by the Young's modulus E and the Poisson ratio γ .

To consider the large deformation of elastic body, the rate of stress $\frac{d^J s_{ij}}{dt}$ is introduced.

$$\frac{d^J s_{ij}}{dt} = G(\dot{\epsilon}_{ij} - \frac{1}{3} \text{tr}(\dot{\epsilon}) \delta_{ij}) \quad \left(G = \frac{E}{2(1+\gamma)} \right) \quad (6)$$

where G is the modulus of elasticity,

$\frac{d^J s_{ij}}{dt}$ is called as the Jaumann derivative which means the rate of stress tensor in a reference frame being corrected according to the rotational effect:

$$\frac{d^J s_{ij}}{dt} = \dot{s}_{ij} + s_{ik} \Omega_{kj} + s_{kj} \Omega_{ik} \quad (7)$$

where Ω_{ij} is an antisymmetric rotation tensor.

The above equations are discretized using the hexahedron element proposed in a classical FVM[9] The both velocity and displacement are defined at the grid points constructing the hexahedron element, and stress is defined at the center of the element.

Numerical Scheme for FSI Problem

In the present study, we propose the weak-coupling method for FSI. Therefore the numerical scheme should be prepared for each of structure and flow field. For the flow computation, the governing equation for unsteady incompressible viscous flow in Cartesian coordinates system are as follows:

$$\frac{\partial u_i}{\partial x_i} = 0 \quad (8)$$

$$\frac{\partial u_i}{\partial t} + \frac{\partial u_i u_j}{\partial x_j} = -\frac{1}{\rho} \frac{\partial p}{\partial x_i} + \frac{1}{Re} \frac{\partial^2 u_i}{\partial x_j \partial x_j} \quad (9)$$

where, Re is Reynolds number. The momentum equations are discretized using the Crank-Nicolson method for the viscous term and the second-order Adams-Bashforth method for convective terms. The temporal discretization is performed with the fractional-step method (Kim et al.[3]):

The spatial discretization is performed with a second-order central difference scheme. The staggered grid system is employed.

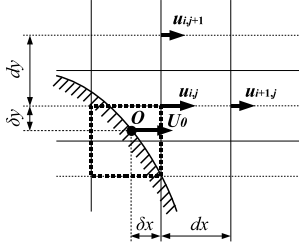


Figure 1: Schematic of interpolation scheme for velocity component

In the flow computation, the interface between fluid and structure is tracked using immersed boundary (IB) method. In the IB method, to represent a boundary on the Eulerian grid, the external force is imposed at the boundary of the flow field so that the boundary velocity satisfies a specified value. The original concept was proposed by Paskin[4]. However, it is well-known the shortcoming, in which the time step should be considerable small compared to the usual one being decided by a CFL condition[2]. To avoid this problem, we introduce the improved IB method called as 'direct forcing method' proposed by Fadlun[2]. In the present study, further in order to easily express an object of arbitrarily shape, the material point is introduced. As shown in figure 1, for a two-dimensional problem, the velocity at the grid point in the vicinity of the wall, u_{ij} is approximated with both the wall velocity, U_0 and the velocity at the slightly distance from the wall, $u_{i+1,j}$ and $u_{i,j+1}$. Thus the relation between these points is as follows:

$$u_{i,j}^{n+1} = aU_0 + bu_{i+1,j}^{n+1} + c_{i,j+1}^{n+1} \quad (10)$$

where the coefficients are geometrically-determined[7].

Calculation Conditions

The computational volume is embedded with two-parallel walls as shown in figure 2. No slip condition is enforced on the both upper and lower boundary. A cylinder is placed on the lower boundary. At the left-side boundary a fully-developed turbulent inflow is produced by a turbulent channel flow computation in which its computational volume, $2h \times \pi h \times 2\pi h$ (h : channel half width) and its grid number, $n_x \times n_y \times n_z = 128 \times 128 \times 100$ are set. The Reynolds number defined with friction velocity, $w_\tau \left(= \sqrt{v \frac{\partial w}{\partial y} |_{y=0}} \right)$ is $Re_\tau = (w_\tau h / \nu) = 150$. At the right-side boundary, a convective outflow boundary is used. Periodicity is enforced in spanwise direction. The grid size is $n_x \times n_y \times n_z = 128 \times 80 \times 128$ in x , y and z directions. The dimension of computational domain is $H_x \times H_y \times H_z = 2h \times \pi h \times 4h$. The cylinder is equipped at the distance $0.25H_z$ from the inlet, and its dimension is $h \times 0.1h \times 0.1h$ and its grid number, $52 \times 12 \times 12$. The non-dimensionalized Young's modulus of elastic cylinder is 250.

Results and Discussions

Instantaneous Vortical Structures

Figures 3 show the instantaneous vortical structure. In the figures, the coherent vortices (white color) are visualized using the isosurfaces of the second invariant of velocity gradient tensor, Q . Since a high threshold value is set, strong vortex structures are captured and distribute in the wake of the cylinder. In general, it is well known that quasi-streamwise vortices govern near-wall turbulence, not show here, we have confirmed that the quasi-streamwise vortices near the wall exist when the threshold of Q value is set as low. Also it can be seen that the ef-

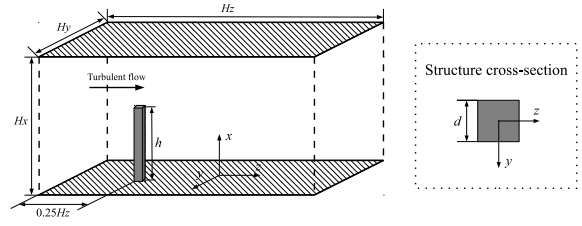


Figure 2: Computational domain for the turbulent channel with a cylinder

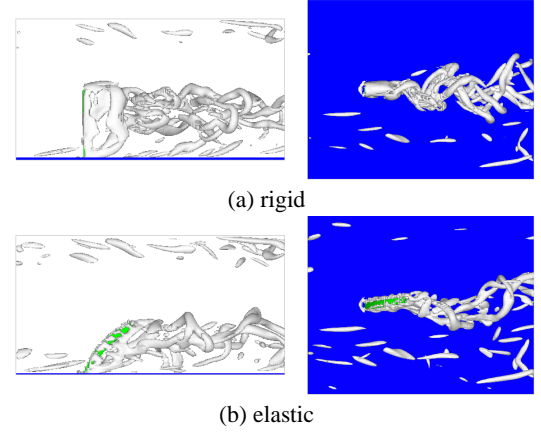


Figure 3: Instantaneous vortical structures (left: side view; right : top view)

fect of cylinder on the instantaneous flow structures is limited around the wake region. For the rigid cylinder (figure 3(a)), the shear layer formed along the span of cylinder is alternately issued from the cylinder and then changes into a hairpin vortex being vertically formed downstream, while for the elastic cylinder (figure 3(b)) the separated shear layer changes into a hairpin vortex being horizontally formed. Not shown here, the periodicity of vortex shedding in the wake of the cylinder are confirmed based on the animations. Further for the elastic cylinder, it is confirmed that the separated shear layer from the cylinder develops both wall-normal and spanwise directions and then evolves into a hairpin vortex, according to the oscillating motion of cylinder.

Vortex Shedding Frequency

The result of FFT (fast Fourier transform) analysis about time signal of the streamwise velocity in the wake at a given position where strong vortical structures are observed. From figure 4(a), a dominant shedding frequency f_s normalized with u_τ and h appears at $f_s = 15.6$ corresponding to the Strouhal number ($St = f_s d / W_m$; W_m : bulk mean velocity at the inflow, $W_m = 15$; $d = 0.1h$), 0.104. This value is good agreement with $St = 0.1$ of experimental data, in which a square cylinder at aspect ratio $h/d = 10$ is immersed within a moderate Reynolds number of turbulent boundary layer flow[5]. From figure 4(b), the Strouhal numbers of elastic cylinder is $St = 0.042$ and converts into the vortex shedding frequency f_s is 6.32 which corresponds to the spanwise vibration period of the elastic cylinder $f_{st} = 6.03$. And as another feature, a resonant frequency of bending primary mode, 5.36 is close to the value of vibration period, f_{st} .

Mean Flow Properties

The mean velocity vectors and two-dimensional streamlines defined with wall-normal and spanwise velocity components are shown in figures 5 In figure 5(a), two vortex pairs with a focus

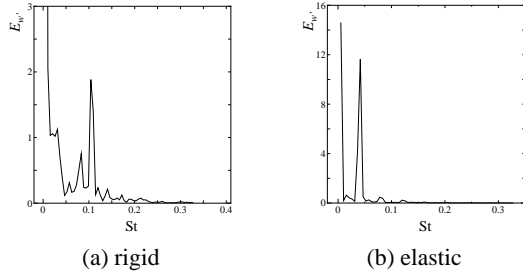


Figure 4: Vortex shedding frequency

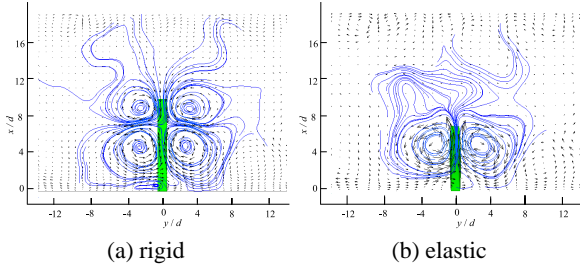


Figure 5: Mean streamlines and velocity vectors on the $x - y$ plane

on the saddle point ($x/d = 7.0, y/d = 0$) are formed. The lower vortex pair entrains an ambient fluid and form an upwash flow from the lower wall, similarly the upper vortices entrains the ambient fluid and form a downwash flow. The lower vortices called as "base vortex"[8] are formed depending on boundary layer thickness of both sides of cylinder. In particular, as a boundary layer thickness becomes thicker, the upwash flow induced by base vortex is enhanced[8]. In the elastic case (figure 5(b)), a single vortex pair is formed and the upwash flow from the lower wall occurs only.

Heat Transfer Characteristics

With regard to the boundary conditions, both an uniform temperature at the inflow and an uniform heat flux on the lower wall are imposed. The contour of mean temperature on $x - y$ plane is shown in figure 6. As can be seen, high temperature region due to uniform heat flux extends over the lower wall. on the other hand different features between elastic and rigid cylinder exist: for rigid cylinder (figure 6(a)), the upwash and downwash flow induced by lower and upper vortex pair contribute to the temperature distribution, i.e., slightly higher temperature distribution than the surroundings extends over the lower wall; for the elastic cylinder (figure 6(b)), the upwash flow due to a single vortex pair contributes to the heat transfer over the lower wall, high temperature region strongly penetrates into the upper region. Figures 7 show the contour of Nu number on the $y - z$ plane. As can be seen, high Nu number region is formed around the both cylinder. The reason why the high temperature occurs is that the well-known "neckless" vortex[8] being formed around the cylinder root induces downwash flow. Further for the rigid cylinder (figure 7(a)) high Nu number region extends in the wake of cylinder, indicating that the quasi-streamwise vortices being actively generated in the low speed region of wake, enhances the heat transfer of this region, while for the elastic cylinder (figure 7(b)), since the spanwise oscillating motion due to elastic cylinder sweeps the wake of cylinder, the homogeneous distribution of Nu number is formed in the wake. From the above mentioned results, although the different feature on heat transfer characteristics between rigid and elastic cylinder emerges in the center of flow passage, however, the influence of

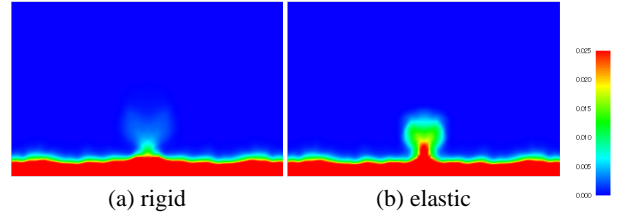


Figure 6: Contour of mean temperature on $x - y$ plane

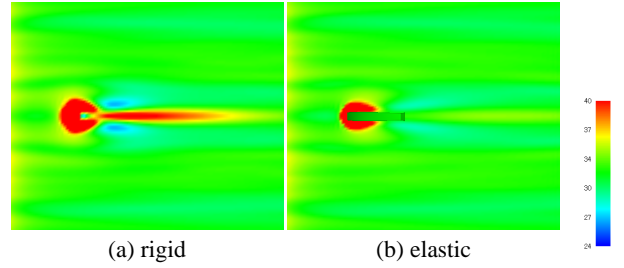


Figure 7: Contours of Nu number on $x - z$ plane

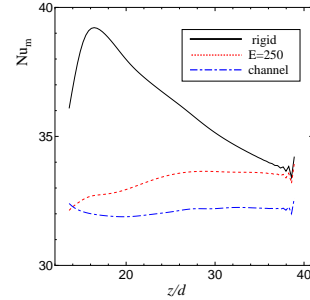


Figure 8: Mean Nusselt number

the cylinder on the heat transfer is limited in the wake of cylinder. In order to quantitatively evaluate the heat transfer performance, the streamwise distribution of Nu number along the line through $x = y = 0$ is shown in figure 8. Compared to the case without cylinder (in the figure "channel"), it is confirmed that the cylinder enhances the heat transfer performance in the wake of cylinder. The Nu number distribution of rigid cylinder denotes a high value behind the cylinder and rapidly decreases downstream. Unlike the rigid cylinder, the elastic cylinder denotes the relatively uniform distribution without the peak value.

Mixing Characteristics

In order to evaluate the improvement of mixing performance due to the elastic cylinder, two cases of passive scalar (ϕ) distribution at inflow are examined as shown in figures 9. To examine the wall-normal mixing, the inflow condition (case (a)) is that in the rectangular region defined with $1/8H_x - 3/8H_x$ scalar (temperature) is unity, other region scalar (temperature) is zero. Also the spanwise mixing is examined using another inflow condition (case(b)).

Figures 10 show the contour of mean scalar on the $x - y$ plane under the condition (a) and (b). As well as the above mentioned heat transfer characteristics, the scalar distributes in the limited region. The mixing features are dominated by vortical structures, i.e., for the rigid cylinder the downwash and upwash flow induced by upper and lower vortex pair contribute to the formation of mixing; for the elastic cylinder the upwash flow due to a single vortex pair governs the mixing characteristics.

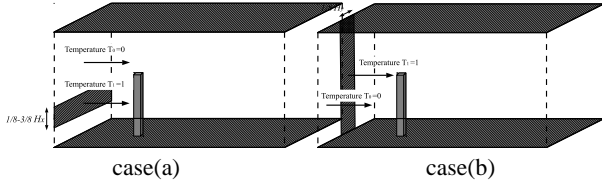


Figure 9: Boundary condition of scalar field

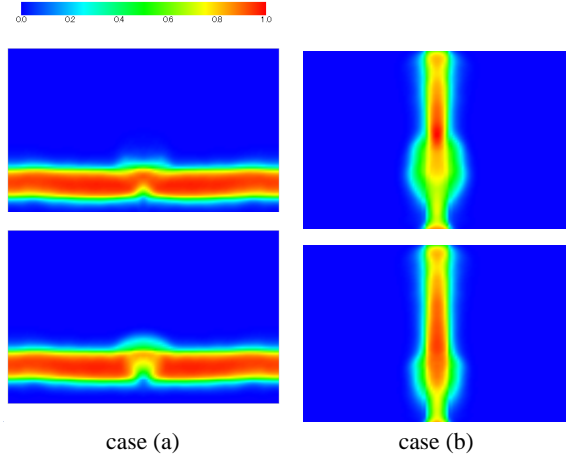


Figure 10: Mean scalar field on the $x - y$ plane (upper: rigid; lower: elastic)

Everson et al.[1] investigated the statistical entropy based on the passive scalar concentration, and they demonstrated the characteristics of this measure by examining the experimental data. And we validate this mixing measure based on the DNS data of active controlled jet[6]. In the following, we provide a simple explanation of this measure. Boltzmann proposed the statistical entropy, which is defined as the logarithm of combination, W .

$$S = k \ln W \quad (11)$$

where k is the Boltzmann constant. W is the combination of the number of molecules in the i -th coarse-grained cell, N_i , namely, $W = \frac{N!}{N_1!N_2!\dots N_M!} = \frac{N!}{\prod N_i!}$. Considering the small volume surrounding a grid point i , $\Delta V (= \Delta_x \Delta_y \Delta_z)$, the number of molecules is denoted by $N_i = \phi_i \Delta V$; therefore,

$$S = k \Delta V \left[\Phi \ln \Phi - \sum_{i=1}^M \phi_i \ln \phi_i \right] \quad (12)$$

where $\Phi = \sum \phi_i$

In order to investigate the streamwise variation of the statistical entropy, S is summed over the plane perpendicular to the streamwise direction, and \bar{S} is defined as S normalized with the inflow quantity, S_0 . M represents the number of grids on the $x - z$ plane.

Under the condition (a), the statistical entropy of rigid cylinder increases near the cylinder and then decreases downstream, while for the elastic cylinder the feature near the cylinder is similar to the rigid cylinder, but unlike the rigid cylinder the statistical entropy is maintained at high level downstream. As well as condition (a), for the condition (b) the statistical entropy of both rigid and elastic cylinder increases around the cylinder and then decreases downstream, however, the elastic cylinder still preserves a higher value of statistical entropy than the rigid cylinder. These findings suggest that the elastic cylinder contributes to the improvement of mixing performance.

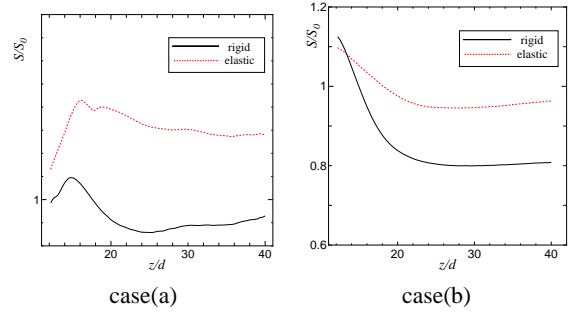


Figure 11: Streamwise entropy distribution

Conclusions

In order to investigate the possibility of flow control using an elastic cylinder, we conduct a simulation of a finite-length elastic cylinder installed in a turbulent channel flow using the proposed FSI scheme. Conclusions are as follows:

- Depending on the profile of cylinder, it is found that vortical structures behind cylinder are formed, i.e., according to the elasticity, the hair-pin vortices are vertically or horizontally formed, respectively.
- Compared to the channel flow without cylinder, the heat transfer performance on the wall of both rigid and elastic cylinder is improved, in particular, the rigid cylinder is capable of enhancing more heat transfer. On the other hand, for the mixing performance further away from the wall, the elastic cylinder is superior to the rigid cylinder.

References

- [1] Everson, R., Manin, D. and Sirovich, L., Quantification of Mixing and Mixing Rate from Experimental Observations, *AIAA J.*, **36**, 1998, 121-127.
- [2] Fadlun, E.A., Verzicco, R., Orlandi, P., and Mohd-Yusof, J., Combined Immersed-Boundary Finite-Difference Methods for Three-Dimensional Complex Flow Simulations, *J. Comp. Physics*, **161**, 2000, 35-60.
- [3] Kim, J., and Moin, P., Application of a fractional step method to incompressible flows, *J. Comp. Physics*, **59**, 1985, 308-323.
- [4] Peskin, C.S., The fluid dynamics of heart valves: Experimental, theoretical and computational methods, *Ann. Rev. Fluid Mech.*, **14**, 1981, 235-259.
- [5] Sakamoto, H., and Arie, M., Vortex shedding from a rectangular prism and a circular cylinder placed vertically in a turbulent boundary layer, *J. Fluid Mechanics*, **126**, 1983, 147-165.
- [6] Tsujimoto, K., Kariya, S., Shakouchi, T. and Ando, T., Evaluation of jet mixing rate based on DNS data of excitation jets, *Int. J. Flow Control*, **1-3**, 2009, 213-225.
- [7] Tsujimoto, K., Kito, A., Shakouchi, T. and Ando, T., Development of Numerical Scheme on Fluid-Structure Interaction for a Flexible Object, *Proc. Int. Conf. Multiphase Flow 2010*, 2010, CDR0M pp.1-9.
- [8] Wang, H. F. and Zhou, Y., HOU, The finite-length square cylinder near wake, *J. Fluid Mech.*, **638**, 2009, 453-490.
- [9] Wilkins, M. L., *Computer Simulation of Dynamic Phenomena*, Springer Verlag GmbH, 2006, 371-390.